

COST-DRIVEN MULTIDISCIPLINARY FRAMEWORK FOR WINGLET DESIGN: A REGIONAL AIRCRAFT CASE STUDY

Luca Falcone[1], Salvatore Corcione[1], Fabrizio Nicolosi[1] & Salvatore Trepiccione[1]

[1]University of Naples Federico II, Department of Industrial Engineering, Via Claudio, 21, Napoli, 80125, Italy

Abstract

Winglets are widely adopted on medium- and long-range transport aircraft, whereas their application to regional aircraft remains comparatively limited. This is not necessarily due to the absence of local aerodynamic benefit, but rather to the presence of a multidisciplinary trade-off in which structural mass penalties, mission characteristics, manufacturing complexity, and maintenance implications may offset the reduction in induced drag. This work presents an integrated, cost-driven framework for the assessment of winglet geometries applied to a hybrid-electric regional aircraft wing. The proposed approach combines aerodynamic analyses performed for representative climb and cruise conditions, structural sizing, component-level wing mass estimation, hybrid-electric mission performance evaluation, and an economic assessment based on direct operating cost. Rather than targeting aerodynamic optimality alone, the framework quantifies how aerodynamic gains propagate to aircraft-level performance and cost metrics, thereby supporting the identification of the mission and economic conditions under which a winglet installation becomes justifiable.

Keywords: Winglet Design, Regional Aircraft, Multidisciplinary Framework, Cost-driven Assessment.

1. Introduction

The reduction of induced drag through the modification of the spanwise lift distribution represents the primary aerodynamic rationale behind the adoption of winglets on fixed-wing aircraft. Their aerodynamic benefits have been extensively documented through both high-fidelity simulations and reduced-order models, with numerous studies showing a strong dependence of the achievable performance on the geometric parameters of the device. As a consequence, single- and multi-objective optimization approaches have been successfully applied to winglet design, often reporting notable drag reductions and improvements in lift-to-drag ratio at the design point [1, 2].

From a structural standpoint, however, the introduction of a winglet alters the wing load distribution and increases the root bending moment, with a direct impact on structural sizing and on the resulting wing mass. Aerostructural and multidisciplinary design studies have repeatedly shown that neglecting the structural penalty associated with the device may lead to overly optimistic conclusions on its actual effectiveness, especially when the constraint of preserving the original wingspan is enforced [3, 4, 5]. Similar aircraft-level studies on unconventional lifting surfaces have also shown that low-fidelity, traceable aero-structural models can be used at conceptual-design level to quantify how elastic efficiency and structural layout changes propagate to mission fuel burn [6].

A further layer of complexity is added when the analysis is extended to mission performance and to the operational economics of the aircraft. Several studies have demonstrated that aerodynamic performance metrics alone are insufficient to capture the actual value of a winglet installation, since manufacturing, installation, and maintenance costs can significantly influence the lifecycle profitability of the modification [7, 8]. In particular, it has been shown that the use of winglets on a Boeing 747-class long-range aircraft could lead to a reduction of approximately 3.8% in fuel weight and of about

https://doi.org/10.71945/icas2026_0783

29 M$ in direct operating cost (DOC) over a 15-year period [9]. While these results clearly illustrate the potential economic impact of winglet integration, they are derived for large, long-range transport aircraft, whose operational profiles, structural characteristics, and cost drivers differ substantially from those of regional platforms.

Regional aircraft are characterized by short cruise segments, high frequency of flight cycles per year, smaller wingspans, and a cost structure in which the fuel-saving potential of an aerodynamic device must be weighed against structural mass, maintenance implications, and aircraft-level operating costs. Previous work on innovative turboprop configurations has therefore coupled aircraft performance and DOC evaluation to compare regional turboprop concepts with regional-jet references, while subsequent wind-tunnel investigations on three-lifting-surface regional transports have highlighted the importance of configuration-level aerodynamic interference and stability validation [10, 11]. More recently, AGILE 4.0 applications to more-electric regional aircraft have further shown the relevance of treating aircraft sizing, electrified on-board systems, mission performance, and certification-related constraints within an integrated multidisciplinary analysis [12]. As a result, the economic justification of a winglet on this class of aircraft cannot be inferred directly from results obtained on long-range platforms; a dedicated, cost-driven assessment is required, in which all the disciplines that contribute to the trade-off are evaluated consistently and on the same configuration.

In this context, the present work re-examines the role of winglets for regional aircraft from a cost-driven multidisciplinary perspective. Rather than evaluating winglets only on aerodynamic grounds, an integrated framework is adopted to capture, in a consistent manner, their effect on aerodynamics, structural sizing, mission performance, and economic metrics. The objective is to assess whether the potential aerodynamic benefits of winglets can be translated into a meaningful aircraft-level economic advantage for a hybrid-electric regional turboprop when all the relevant disciplines are considered simultaneously.

The remainder of the paper is organized as follows. Section 2. describes the integrated workflow and its individual disciplinary modules: input data and reference aircraft, flight envelope, geometry parametrization, aerodynamics, wing mass estimation, mission performance, and cost assessment. Section 3. presents the results obtained from the application of the workflow to the reference hybrid-electric regional turboprop, including the trends observed across the winglet design space and the corresponding mission-level economic outcome. Section 4. summarizes the main findings and outlines possible directions for future work.

2. Integrated framework overview

The proposed methodology, illustrated in Figure 1, is based on a Design of Experiments (DOE) applied to the winglet geometry, embedded in a sequential, tightly coupled framework. This organization is consistent with previous parametric aircraft-design environments and collaborative model-based multidisciplinary design analysis and optimization (MDAO) frameworks developed for conceptual and preliminary design, where modular disciplinary analyses, DOE campaigns, and optimization loops are used to explore aircraft-level design spaces with performance, mass, environmental, and DOC metrics [13, 14, 15]. For each candidate configuration, geometry generation, aerodynamic analysis, structural sizing, wing mass estimation, mission performance evaluation, and economic assessment are executed in a consistent and repeatable manner, sharing a common set of input data and design loads.

The framework is organized in seven logical blocks, executed sequentially within each DOE iteration:

1. **Input data**: definition of the reference aircraft, of the structural and material properties, and of the bounds of the design variables;
2. **Flight envelope**: construction of the manoeuvre and gust V-n diagrams, and identification of the design load condition;
3. **Geometry**: generation of the wing-plus-winglet geometry under iso-area and iso-span constraints, with continuous blending between wing and winglet;
4. **Aerodynamics**: panel-method analyses for representative climb and cruise conditions, with extraction of polar coefficients and spanwise load distributions;

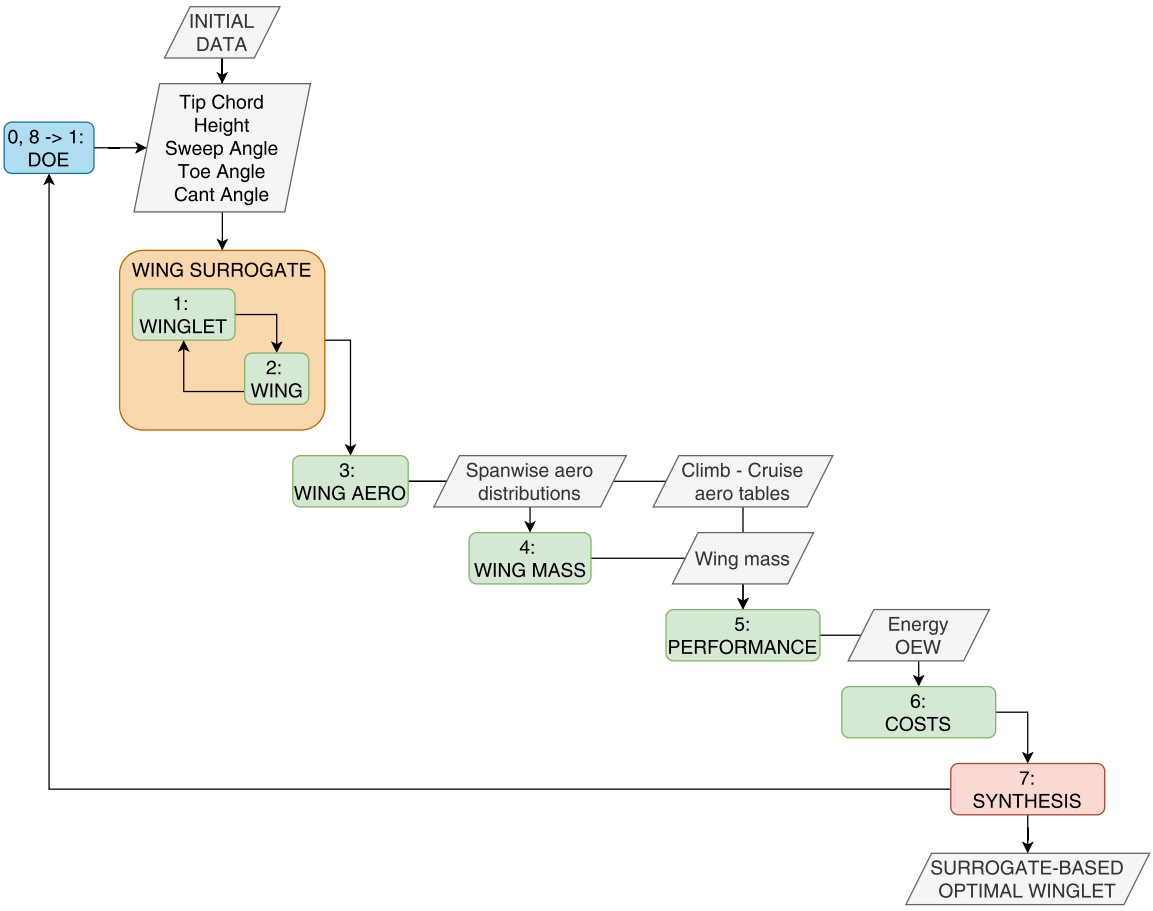


Figure 1 – Integrated cost-driven framework for winglet design assessment.

5. **Wing mass**: structural sizing driven by the design loads and by the spanwise aerodynamic distributions;

6. **Performance**: mission simulation on a typical regional profile, in which the aerodynamic and structural effects of the winglet are translated into aircraft-level fuel consumption and mass-related performance metrics;

7. **Costs**: economic assessment of the configuration through a DOC model including capital, crew, energy, fees and charges, and maintenance contributions, driven by the modified aircraft mass and mission fuel consumption.

The DOE design variables governing the winglet geometry are the tip chord $c_{tip,w}$, the toe angle τ_w, the winglet height h_w, the sweep angle Λ_w, and the cant angle ϕ_w. A graphical definition of these variables is given in Figure 2, while the corresponding ranges spanned by the DOE are listed in Table 1. The winglet root chord, and therefore the resulting taper ratio, is not an independent variable: it is implicitly determined by the geometric continuity requirement at the wing-winglet junction and by the iso-area, iso-span constraint applied to the complete wing-plus-winglet planform.

Table 1 – DOE design variables and bounds.

Design variable	Symbol	Range	Levels
Tip chord (m)	$c_{tip,w}$	$[0.25,\ 0.45]$	3
Toe angle (deg)	τ_w	$[-9,\ 0]$	4
Height (m)	h_w	$[0.50,\ 1.50]$	3
Sweep angle (deg)	Λ_w	$[25,\ 45]$	2
Cant angle (deg)	ϕ_w	$[55,\ 85]$	3

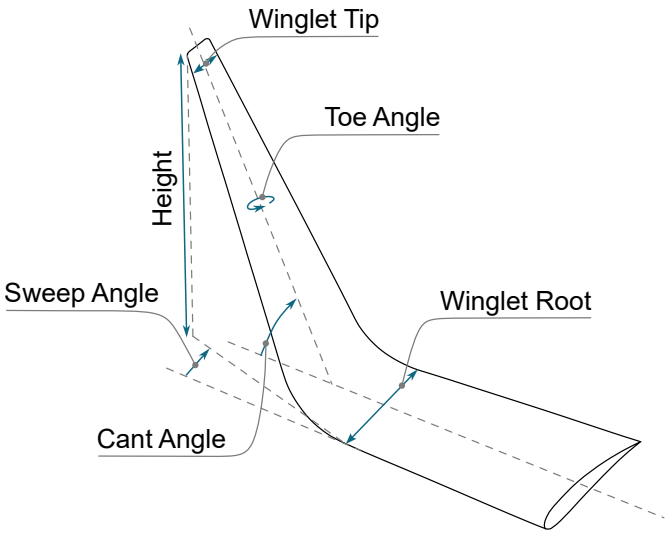


Figure 2 – Parametric definition of the winglet geometry adopted in the Design of Experiments.

The baseline configuration (wing without winglet) is analyzed once, providing the reference for all subsequent comparisons. Each DOE iteration then yields a self-consistent set of geometric, aerodynamic, structural, performance, and economic figures of merit, which are stored and made available to the synthesis stage. The DOE database is then used to rank the explored configurations and to identify the regions of the design space that offer the most favourable compromise.

2.1 Input data

The reference platform adopted in this study is a regional turboprop aircraft derived from a next-generation hybrid-electric conceptual architecture developed within the HERA (Hybrid Electric Regional Aircraft) project, part of the European Clean Aviation programme and targeting mid-2030s entry into service. The HERA configuration is sized for short- to medium-range missions and incorporates advanced wing designs, innovative airframe solutions and low-emission propulsion concepts. In the present framework, the hybrid-electric nature of the platform is retained in the mission-performance analysis.

The main mass and operational limits of the reference aircraft, used in the construction of the flight envelope and in the structural sizing, are summarized in Table 2 in terms of maximum take-off weight (MTOW), maximum landing weight (MLW), maximum zero-fuel weight (MZFW), and operating empty weight (OEW). The wing planform is defined by two trapezoidal panels: Panel 1 spans from the root to the kink station and adopts a NACA 23018 profile throughout; Panel 2 extends from the kink to the tip and transitions linearly to a NACA 23015 at the wingtip. The planform parameters of each panel are reported in Table 3.

Table 2 – Reference aircraft: operational limits and masses.

Item	Value
MTOW (kg)	27000
MLW (kg)	25000
MZFW (kg)	23000
OEW (kg)	18600
Z_{MO} (ft)	25000
M_{MO} (–)	0.55

Table 3 – Reference wing: panel definition.

Item	Panel 1	Panel 2
Span (m)	4.75	11.75
Root chord (m)	2.574	2.574
Tip chord (m)	2.574	1.100
Tip twist (deg)	0	-2
Dihedral (deg)	0	2.5
LE sweep (deg)	0	1.72

The wing structural model is based on a single-cell box representation, with front and rear spars located at 25% and 70% of the local chord, respectively. For each DOE configuration, the primary wing mass is first obtained from the structural sizing procedure described in Section 2.5. The final

wing mass is then computed by applying fixed correction factors that account for secondary structures and aeroelastic reinforcements, reported in Table 4. The safety factor adopted for the conversion from limit to ultimate loads is fixed at $sf = 1.5$, as prescribed by CS 25.303 [16].

Table 4 – Fixed correction factors used in the wing-mass build-up.

Parameter	Value	Description
k_{sec} (–)	0.30	Secondary structure mass fraction (of primary)
k_{aero} (–)	0.15	Aeroelastic penalty fraction (of primary)

2.2 Flight envelope

The construction of the flight envelope provides the design load conditions used for the structural sizing. The envelope is constructed at sea level, which represents the most critical condition. In equivalent airspeed the manoeuvre boundary is essentially altitude-invariant, whereas the derived gust velocities prescribed by the standard decrease with altitude, so that both the gust boundary and the design speed V_B it fixes are most severe at sea level. The maximum operating Mach number M_{MO} is used to define the upper speed boundary. The overall envelope is composed of a manoeuvre contribution, a gust contribution, and a flight envelope obtained by combining the two.

The *manoeuvre* envelope is constructed by combining the aircraft-specific characteristics with the requirements prescribed by CS 25.337. The positive and negative limit load factors, together with the characteristic speeds and corner points of the V-n diagram, are therefore computed at sea level according to the regulatory definitions using the reference aircraft mass, wing loading, operating-speed limits, and aerodynamic capability. Within the stall-bounded portion of the manoeuvre envelope, the load factor is limited by

$$n_{stall}(V) = \frac{1}{2}\rho V^2 \frac{S_{ref}}{W} C_{Z,max}, \tag{1}$$

which is intersected with the prescribed limit load factors at V_A to define the corner points of the envelope.

The *gust* envelope is not constructed by means of the dynamic gust analyses prescribed by CS-25 (continuous turbulence and discrete gusts aeroelastic simulations); rather, a simplified, quasi-static formulation is adopted, based on the gust load factor of CS 23.341(c) [17], which derives from the Pratt-Walker formulation. The gust load factor at a given equivalent airspeed V_{EAS} is computed as

$$n_{gust} = 1 \pm \frac{k_g \rho_0 V_{EAS} C_{L\alpha} U_{de}}{2\,(W/S)}, \tag{2}$$

where U_{de} is the derived gust velocity prescribed by the standard, $C_{L\alpha}$ is the wing lift-curve slope, and k_g is the Pratt gust-alleviation factor, expressed in terms of the mass ratio μ_g:

$$k_g = \frac{0.88\,\mu_g}{5.3 + \mu_g}, \qquad \mu_g = \frac{2\,(W/S)}{\rho\,\bar{c}\,C_{L\alpha}\,g}. \tag{3}$$

The gust load factor is evaluated at the design speeds V_C and V_D, with the corresponding values of U_{de}, and at two reference altitudes: sea level and the maximum operating altitude $Z_{MO} = 25000$ ft. This simplified formulation is adopted because the flight-envelope evaluation must remain sufficiently fast to be embedded within the DOE, while still providing a regulation-based estimate of the gust loads at the level of fidelity required by a conceptual-design study. If the objective were extended towards a certification-oriented workflow, the regulatory assumptions and their traceability could be treated in a more formal way, for instance through model-based systems engineering (MBSE) digitalization of airworthiness requirements [18].

The manoeuvre and gust contributions are then combined into a single *flight* envelope, whose outer boundary defines the limit load factor as a function of equivalent airspeed. The design point used in the structural sizing is assumed to be the point D, located at V_D and corresponding to the most critical load factor between the manoeuvre and the gust envelopes:

$$n_z^{des} = \max\left(n_{man}(V_D),\, n_{gust}(V_D)\right). \tag{4}$$

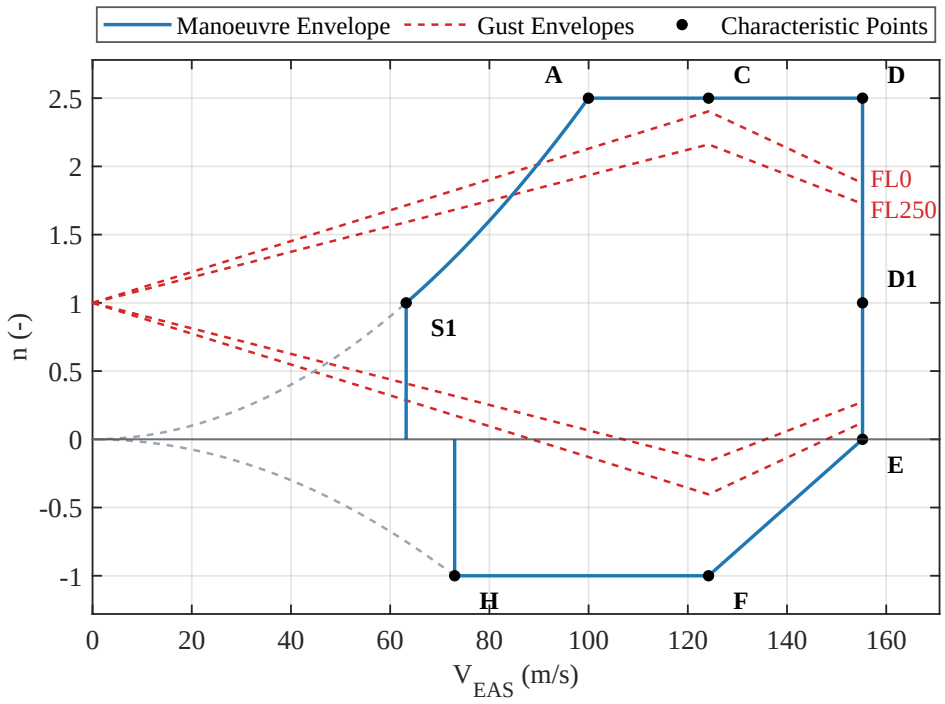


Figure 3 – Combined manoeuvre and gust V-n envelope.

A schematic representation of the resulting manoeuvre and gust envelopes is provided in Figure 3. It should be noted that the actual critical structural load case cannot be identified a priori from the flight-envelope diagram alone, since different combinations of load factor and equivalent airspeed may generate different internal load distributions and therefore different structural demands. A complete search over all possible envelope points is outside the scope of the present work; therefore, point D is retained as the reference critical load case for the structural sizing.

2.3 Geometry

The geometric model of the wing is built starting from the panel definition reported in Table 3. Chord, twist, dihedral, and leading-edge sweep are specified at root, kink, and tip; the corresponding airfoil sections are then interpolated linearly between the assigned breakpoints. The geometry is discretized along the span and along the airfoil contour, providing a surface that can be exported to the aerodynamic solver. The winglet is appended to the wing tip according to the parametric definition shown in Figure 2. The five independent geometric parameters $(c_{tip,w}, \tau_w, h_w, \Lambda_w, \phi_w)$ define the sampled design space.

In order to ensure that the aerodynamic and structural comparisons among different winglet configurations are not biased by changes in the global wing planform, the reference area S_{ref} and the wing span b — and consequently the aspect ratio AR — are kept constant across all DOE configurations:

$$S(\mathbf{x}) = S_{ref}, \qquad b(\mathbf{x}) = b_{ref}, \qquad AR = \frac{b_{ref}^2}{S_{ref}} = \text{const}, \tag{5}$$

where $\mathbf{x}$ collects the winglet design variables. The constraint of Equation 5 requires a minor geometric adjustment of the baseline wing whenever a winglet is appended: the chord of the wing tip and the span of the outer panel are updated iteratively until both S_{ref} and b_{ref} converge back to the reference values within a prescribed tolerance.

This iso-area, iso-span constraint is instrumental to the methodological consistency of the framework: any change in induced drag, lift-to-drag ratio, or spanwise load distribution can be primarily attributed to the presence of the winglet itself and to the associated modification of the load distribution, rather than to a change in aspect ratio or in reference area. Once the converged geometry is obtained, the wing-plus-winglet surface is exported in the format required by the aerodynamic solver.

2.4 Aerodynamics

The aerodynamic characterization of each configuration is performed by means of a three-dimensional panel method, implemented in the commercial code Altair FlightStream 25.1. The panel method is well suited to the present application, since it provides a computationally efficient estimate of induced drag, lift-to-drag ratio, and spanwise load distribution at a computational cost compatible with the large number of configurations explored within the DOE, while still capturing the three-dimensional flow effects induced by the winglet at conceptual-design level. The converged solution of the lowest-DOC winglet configuration is shown in Figure 4.

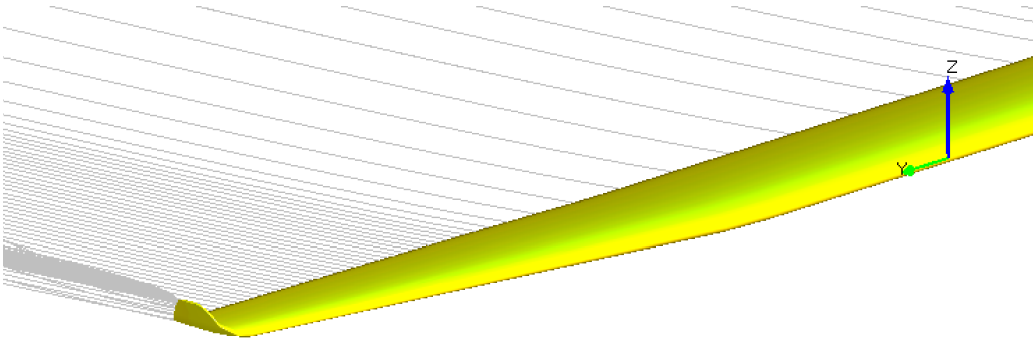


Figure 4 – FlightStream aerodynamic analysis of the lowest-DOC winglet configuration (ID 128).

For each candidate geometry, two flight conditions are simulated, corresponding to the climb and cruise segments of the reference mission. The two conditions differ in atmospheric properties, true airspeed, Mach number, and angle-of-attack range, in order to capture both the behaviours relevant for climb and cruise. The corresponding parameters are summarized in Table 5.

Table 5 – Flight conditions adopted in the aerodynamic analyses.

Item	**Climb**	**Cruise**
True airspeed (m/s)	98.52	158.02
Mach number (–)	0.30	0.50
Air density (kg/m^3)	0.9046	0.6527
Static pressure (Pa)	69682	46563
Temperature (K)	268.34	248.53
Angle of attack range (deg)	$5 \rightarrow 10$	$0 \rightarrow 6$

For each condition, an angle-of-attack sweep is performed over the prescribed range. From the resulting polar, the zero-lift drag coefficient C_{D0} and the induced-drag factor k in the parabolic approximation

$$C_D = C_{D0} + k C_L^2 \tag{6}$$

are extracted by least-squares fitting. The corresponding Oswald efficiency factor e and maximum lift-to-drag ratio $(L/D)_{max}$ are then derived from the standard relations

$$e = \frac{1}{\pi AR k}, \qquad \left(\frac{L}{D}\right)_{max} = \frac{1}{2\sqrt{C_{D0}\, k}}. \tag{7}$$

These four scalar metrics provide a compact yet representative description of the aerodynamic behaviour of the configuration in each of the two flight conditions.
In addition to the integral coefficients, the panel-method analyses provide the spanwise distribution of sectional aerodynamic forces and pitching moment along the wing-plus-winglet surface. These

distributions provide the spanwise shape of the running loads acting on the wing, whose magnitude is subsequently rescaled to the design load condition within the structural sizing module. This behaviour is illustrated in Figure 5, where the spanwise load distribution, normalised as $c_n c/c_{av}$, of the baseline wing is compared with the lowest-DOC and highest cruise lift-to-drag ratio winglet configurations.

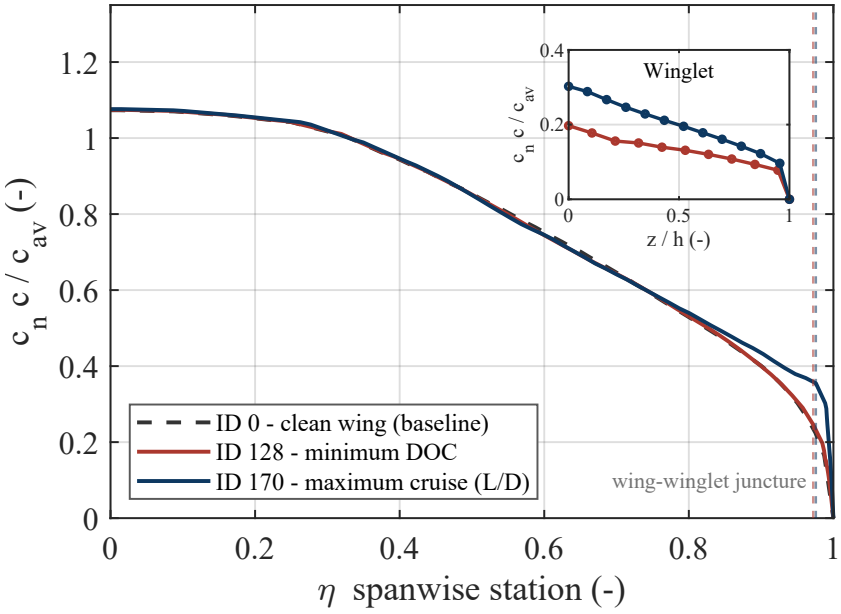


Figure 5 – Spanwise load distribution $c_n c/c_{av}$ at $\alpha = 6°$ for the baseline wing (ID 0), the lowest-DOC winglet configuration (ID 128), and the configuration with the highest cruise lift-to-drag ratio (ID 170).

The dashed vertical lines mark the wing-winglet juncture of each device, in the colour of its own curve. The winglet load is plotted against its own normalised height z/h, measured from the juncture.

2.5 Wing mass

The structural mass of the wing is estimated by means of a simplified box-beam representation, sized at the design load condition derived from the flight envelope (Section 2.2). The wing primary structure is idealized as a single-cell box, bounded by the front and rear spars — located at 25% and 70% of the local chord, respectively — and by the upper and lower skins. The structural layout and material assumptions are kept fixed throughout the DOE.

The wing is discretized along the semi-span, and at each station the internal shear force $V(y)$, bending moment $M(y)$, and torsional moment $T(y)$ are computed by integrating the running loads obtained from the aerodynamic analysis, scaled by the design load factor and corrected for the inertial relief of the structure itself and of the distributed wing-mounted items. The local sizing is performed on the basis of the ultimate loads, obtained from the limit loads as

$$\mathbf{L}_{ult} = sf \cdot \mathbf{L}_{lim}, \qquad sf = 1.5, \tag{8}$$

where $\mathbf{L}$ denotes the vector of internal load resultants. The resulting stresses are then verified against the yield stress of the material. Based on the internal loads, the primary structural components — upper and lower skin panels, stringers, spar caps, spar webs, and ribs — are sized so that the resulting equivalent stress fulfils a strength criterion under ultimate load conditions.

A set of empirical corrections, consistent with the approach reported in [6], is then applied to the primary structural mass. The total wing mass is computed as

$$M_{wing} = (1 + k_{sec} + k_{aero})\, M_{prim}, \tag{9}$$

where M_{prim} is the primary mass obtained by spanwise integration of the dimensioned components, k_{sec} is the secondary structure mass fraction, and k_{aero} is the aeroelastic penalty fraction.

The procedure is wrapped in an outer convergence loop that ensures consistency between the wing mass used to alleviate the loads and the wing mass returned by the structural sizing. Convergence

is achieved when the relative change in wing mass between two successive iterations falls below a prescribed tolerance. The output of this discipline is therefore a self-consistent wing mass, which enters the mission performance and cost stages as the structural penalty associated with the candidate winglet configuration.

2.6 Performance

The mission performance module translates the disciplinary outputs of the aerodynamic and structural stages into aircraft-level fuel and energy metrics by means of an in-house workflow. The module operates on the full aircraft rather than on the isolated wing, and it couples the wing-specific results produced by the preceding stages with the semi-empirical aerodynamic characterisation of the remaining airframe components and with the propulsive and energy-management representation of the hybrid-electric architecture. The propulsive and energy-management part of the performance module follows the hybrid-electric powerplant formulation developed for regional propeller-driven aircraft [19]. In that formulation, thermal engines, battery systems, and fuel-cell systems are coupled through explicit power-management relationships, enabling rapid and physically consistent mission-level evaluations from the early design stages. The aerodynamic interface between the two levels of fidelity is handled through a table-injection procedure. For each candidate winglet configuration, the climb and cruise polars extracted from the panel-method analyses (Section 2.4) are provided as look-up tables indexed by angle of attack. At runtime, the `AerodynamicsManager` first executes its standard full-aircraft semi-empirical calculation for all components and all flight phases; the main-wing aerodynamic data for climb and cruise are then overwritten by values interpolated from the supplied tables, and the aircraft-level polar assembly is re-executed for these two phases alone, so that the total aircraft aerodynamics consistently reflect the panel-method characterisation of the wing-plus-winglet surface. All other components and flight phases remain unchanged.

The resulting aircraft aerodynamic model, together with the wing mass delivered by the structural sizing (Section 2.5), is passed to the `MissionAnalysisManager`, which simulates a typical regional mission profile comprising taxi, take-off, climb, cruise, descent, and landing, as illustrated in Figure 6. Consistency between the assumed and computed propellant masses is enforced through an outer convergence loop that iterates over the weights, aerodynamics, and mission stages until the relative change in block fuel between successive iterations falls below a prescribed tolerance of 2%. At each iteration, the converged take-off mass is updated accordingly. The loop terminates when both the kerosene and, where applicable, the hydrogen fuel residuals satisfy the convergence criterion simultaneously.

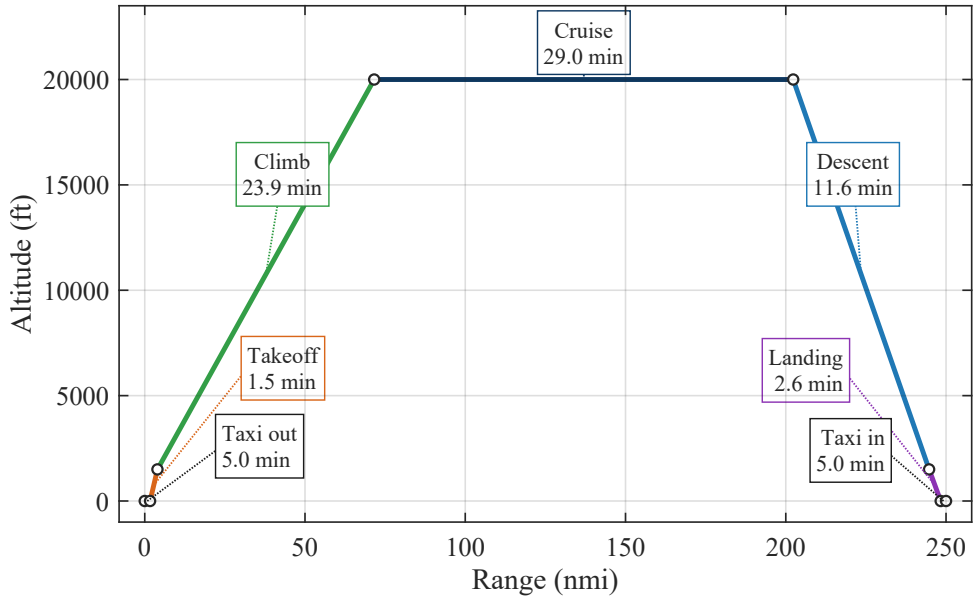


Figure 6 – Simulated regional mission profile, comprising taxi, take-off, climb, cruise, descent, and landing segments.

The primary outputs retained for the winglet assessment are the block fuel, the total electrical energy consumed, and the converged aircraft mass properties—including the updated maximum take-off mass and zero-fuel mass—which are passed directly to the cost module. These quantities capture the net aircraft-level effect of the winglet: the aerodynamic gain may reduce the fuel consumption during the climb and cruise phases, while the structural mass penalty of the sized wing increases the take-off mass and partially offsets this benefit. The net balance between these two competing effects, propagated through the full mission simulation, constitutes the mission-level figure of merit on which the subsequent economic assessment is based. The power split between the thermal and electric propulsion systems throughout the mission, together with the corresponding evolution of the battery state of charge, are shown in Figure 7 and Figure 8, respectively.

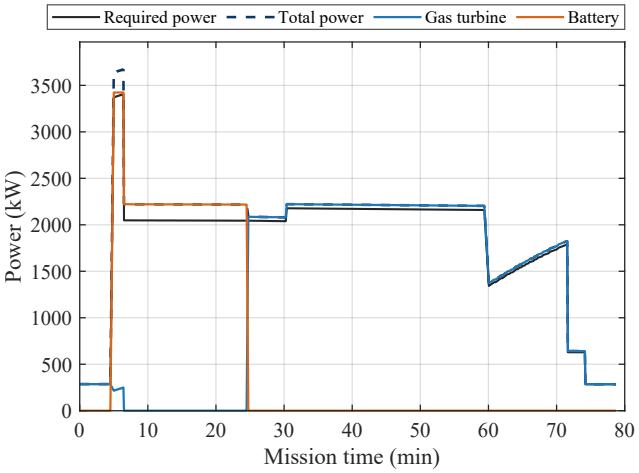


Figure 7 – Power distribution between the thermal and electric propulsion systems over the simulated mission profile.

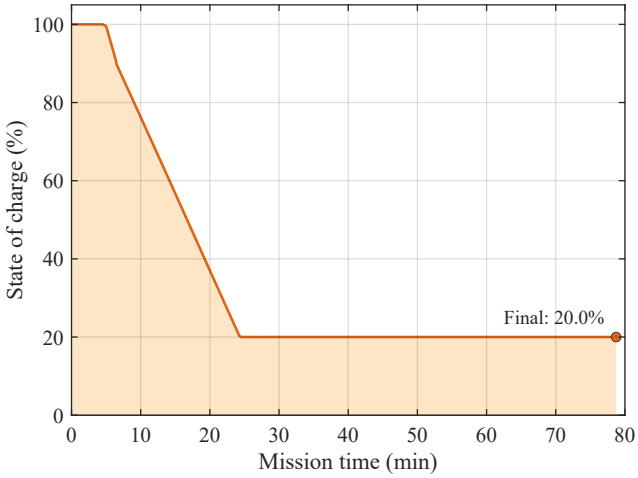


Figure 8 – Battery state of charge evolution throughout the simulated mission profile.

2.7 Direct operating costs

The cost module receives as input the mission-level quantities provided by the aircraft analysis workflow—namely block fuel, block time, block speed, stage length, and the converged mass properties of the candidate configuration, including the mass of the sized wing. These variables are combined with advanced cost-estimating relationships (CERs) to evaluate the aircraft direct operating cost (DOC).

Traditional cost estimation methods often rely on simplified statistical correlations strictly tied to the aircraft MTOW. Such approaches are of limited value for unconventional, retrofitted, or hybrid-electric architectures, whose cost drivers are not captured by the statistical basis on which those correlations were built. In the present work, DOC is treated not merely as a post-processing metric depending on fuel burn, but as an integrated, aircraft-level performance indicator affected by aerodynamic efficiency, structural mass build-up, annual utilization, and operational assumptions following the methodology described in [20]. That work addresses a conventional aircraft and its hybridised derivative, and the present application preserves the same structure, with the conventional ATR 72-600 in the role of the reference aircraft and the hybrid-electric platform in that of the derivative. Method coefficients were left unchanged, while aircraft-specific and operational inputs were replaced with values for the present platform, drawn from published airport and air-navigation tariffs, appraised aircraft values, and published maintenance data for the type.

Moreover, following recent aircraft-retrofit and hybrid-electric cost assessment methodologies [21], the framework strictly segregates capital-related expenditures (CAPEX) from cash operating costs (OPEX). The comprehensive cost breakdown is schematically reported in Figure 9, where green blocks isolate the components specific to the electrified powertrain.

On the CAPEX side, depreciation metrics account for the substantial share of upfront investment required for the battery packs. Unlike conventional assets, aviation-grade battery packs are mod-

eled with a conservative residual value of 25% to account for strict airworthiness standards, weight-optimized housing, and limited secondary-market repurposing opportunities outside the aviation sector. On the OPEX side, the model incorporates a dual-source energy expenditure line, tracking both fossil fuel consumption and net grid electricity consumption. Maintenance costs are similarly decoupled: conventional airframe and thermal engine items follow modified Air Transport Association (ATA) derived standards, with the airframe contribution driven by the airframe mass and therefore responsive to the sized wing, while electric motor subsystems are independently resolved into line (light) and base (heavy) maintenance events based on unique operational frequencies and mean times between maintenance (MTBM). Finally, operational fees encompass terminal air navigation services (TANS), en-route navigation, ground handling charges (GHC), and environmental externalities such as noise and pollutant taxes. The present implementation of this scheme was verified against the reference calculation of [20]: every element—total investment, aircraft and battery depreciation, interest, insurance, crew, fuel, ground handling, terminal and en-route charges—is reproduced to numerical precision.

Within this multidisciplinary framework, the winglet design affects the economic assessment through two coupled paths. First, it alters the aerodynamic efficiency, directly affecting the block fuel and the electric energy required for the mission. Second, it introduces a structural mass penalty, which propagates into the mass-driven airframe maintenance terms and into the mass-dependent airport charges. The remaining contributions, namely capital and crew, are governed by the aircraft delivery price, the annual utilization, and the block time, none of which is altered by the winglet at constant mission and constant block speed. The economic merit of each winglet candidate is therefore assessed through a trade-off between energy savings and structural mass penalties, using aircraft-level DOC as the final filtering metric.

It should be noted that direct operating cost estimates at conceptual design level are indicative of magnitude rather than predictive of an operator's accounts, since several economic inputs—negotiated handling rates, maintenance agreements, financing terms—are commercially confidential; the value obtained here is nevertheless consistent with published figures for aircraft of this class and mission.

3. Results

The DOE campaign comprises the baseline wing and 216 winglet configurations obtained from the combination of the five design variables listed in Table 1. The baseline configuration provides the reference against which all winglet cases are compared. The main aerodynamic, structural, performance, and cost indicators of the baseline are summarized in Table 6. The lowest-DOC winglet configuration is summarized in Table 7; its geometry is shown in Figure 4.

Table 6 – Baseline configuration. The aerodynamic coefficients refer to the isolated wing surface.

Quantity	Value
k_{climb}	0.02075
$(L/D)_{max,climb}$	33.81
k_{cruise}	0.01998
$(L/D)_{max,cruise}$	36.20
Wing mass (kg)	1891.9
Block fuel (kg)	581.97
DOC (€¢/(nm pax))	24.889

Table 7 – Lowest-DOC winglet configuration (case ID 128). The aerodynamic coefficients refer to the isolated wing-plus-winglet surface.

Quantity	Value
Tip chord (m)	0.35
Toe angle (deg)	-9
Height (m)	0.50
Sweep angle (deg)	45
Cant angle (deg)	70
k_{climb}	0.02062
$(L/D)_{max,climb}$	34.93
k_{cruise}	0.01902
$(L/D)_{max,cruise}$	37.12
Wing mass variation	$+1.10\%$
Block fuel variation	-0.858%
DOC variation	-0.036%

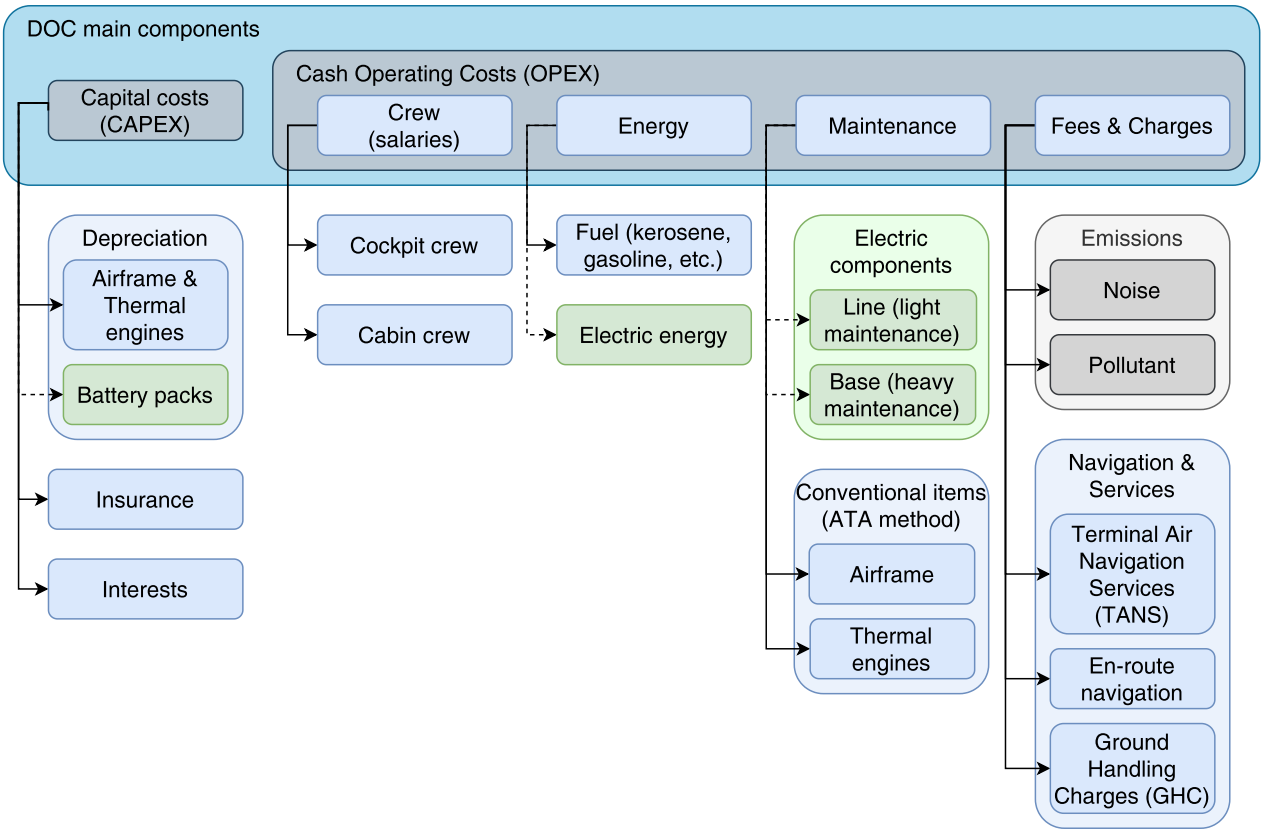


Figure 9 – Breakdown of DOC components adapted from [20]. Green blocks highlight elements specific to a hybrid-electric powerplant.

The composition of the baseline DOC is reported in Table 8. Capital and crew together account for almost half of the total and are identical for the baseline and for every winglet configuration, since neither responds to the wing; the winglet can therefore act only on the remaining share, through the energy, charges and maintenance items.

Table 8 – Breakdown of the baseline direct operating cost.

Item	DOC (€¢/(nm pax))	Share
Capital	8.526	34.3%
Crew	3.025	12.2%
Energy	2.622	10.5%
Airport and en-route charges	6.574	26.4%
Maintenance	4.142	16.6%
Total	24.889	100%

The aerodynamic response of the DOE confirms that winglets can produce local aerodynamic improvements. Relative to the baseline wing, the induced-drag factor is reduced by up to approximately 7.1% in climb and 12.4% in cruise. The corresponding Oswald efficiency factor increases by up to approximately 7.6% in climb and 14.2% in cruise, while the maximum lift-to-drag ratio increases by up to about 6.2% in climb and 4.2% in cruise. These trends show that the explored parametrization is able to generate aerodynamically beneficial winglet shapes within the fidelity limits of the panel-method analysis.

The aerodynamic benefit is not obtained in isolation, however. The winglet modifies the spanwise load distribution, shifts part of the aerodynamic loading outboard, and introduces additional tip loads. These effects increase the structural demand transmitted to the inboard wing and lead to a heavier sized structure throughout the sampled design space. Over the DOE, the wing-mass variation ranges from approximately +0.85% to +8.50%, with an average increase of about 3.33% with respect to the

baseline; no configuration is lighter than the baseline. The structural response therefore offsets a substantial part of the local aerodynamic gain before the configuration is propagated to aircraft-level performance.

At mission level, the combined aerodynamic and structural effects lead to small variations in block fuel and DOC, and the two quantities do not move together. Most of the design space does reduce block fuel with respect to the baseline, but only a small subset of it converts that saving into a lower operating cost, because the structural mass penalty propagates into the mass-driven airframe maintenance and airport-charge terms and absorbs the energy saving. The achievable margin is in any case very limited: the lowest-DOC winglet case reduces block fuel by approximately 0.858% and DOC by approximately 0.036%.

Across the DOE, the block-fuel variation ranges from approximately -0.989% to $+0.562\%$, while the DOC variation ranges from approximately -0.036% to $+0.239\%$. Block fuel is reduced by the large majority of the sampled configurations, whereas 39 cases reduce DOC; the penalty incurred by the least favourable winglet is moreover almost seven times larger than the benefit offered by the best one. The sign and the magnitude of the aircraft-level effect therefore depend on the choice of the geometry rather than on the presence of the device, and an unfavourable choice is considerably more damaging than a favourable one is beneficial.

The trade-off between aerodynamic benefit, structural mass, and operating cost is shown in Figure 10. Each point represents one winglet configuration, with the wing-mass variation on the horizontal axis, the maximum lift-to-drag variation on the vertical axis, and the DOC variation represented by the colour scale. The climb and cruise views are reported side by side in order to separate the two aerodynamic conditions while preserving the same aircraft-level cost metric. The plots show that configurations with improved aerodynamic efficiency do not necessarily provide lower operating cost, because the associated structural and mission-level penalties neutralize the local aerodynamic advantage.

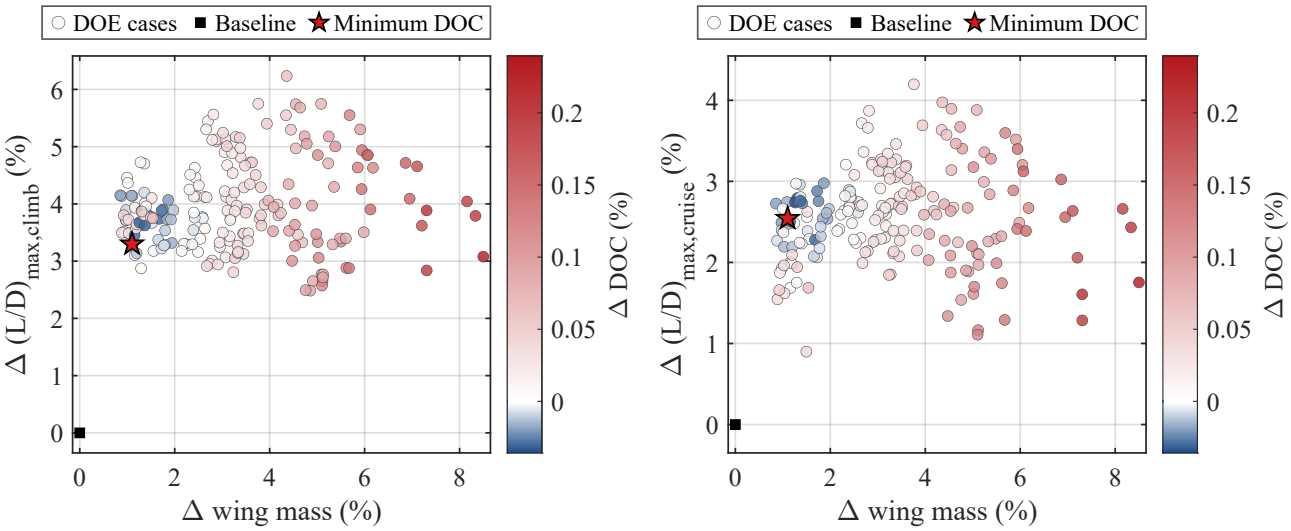


Figure 10 – Trade-off between aerodynamic benefit, wing-mass variation, and DOC variation for the DOE configurations: climb condition on the left and cruise condition on the right.

The influence of the individual design variables on the cost metric is reported in Figure 11. The solid line represents the mean DOC variation associated with each sampled level, while the shaded band indicates the minimum-to-maximum range obtained by varying the remaining parameters. The toe angle is the variable with the largest influence on DOC, with a mean spread of about 0.105% across its levels and a minimum at -9°, followed by the winglet height (0.058%), whose mean DOC variation increases monotonically as the device grows taller. Both effects are monotonic over the sampled range, so the cost optimum lies on the boundary of the explored design space rather than inside it; extending the toe-angle range would be required to locate it, but the associated margin is of the same order as the values discussed above and does not alter the aircraft-level conclusion. The cant angle produces a spread of 0.027%, while the tip chord and the sweep angle produce 0.014% each, and

the three are therefore of secondary importance for the cost metric.

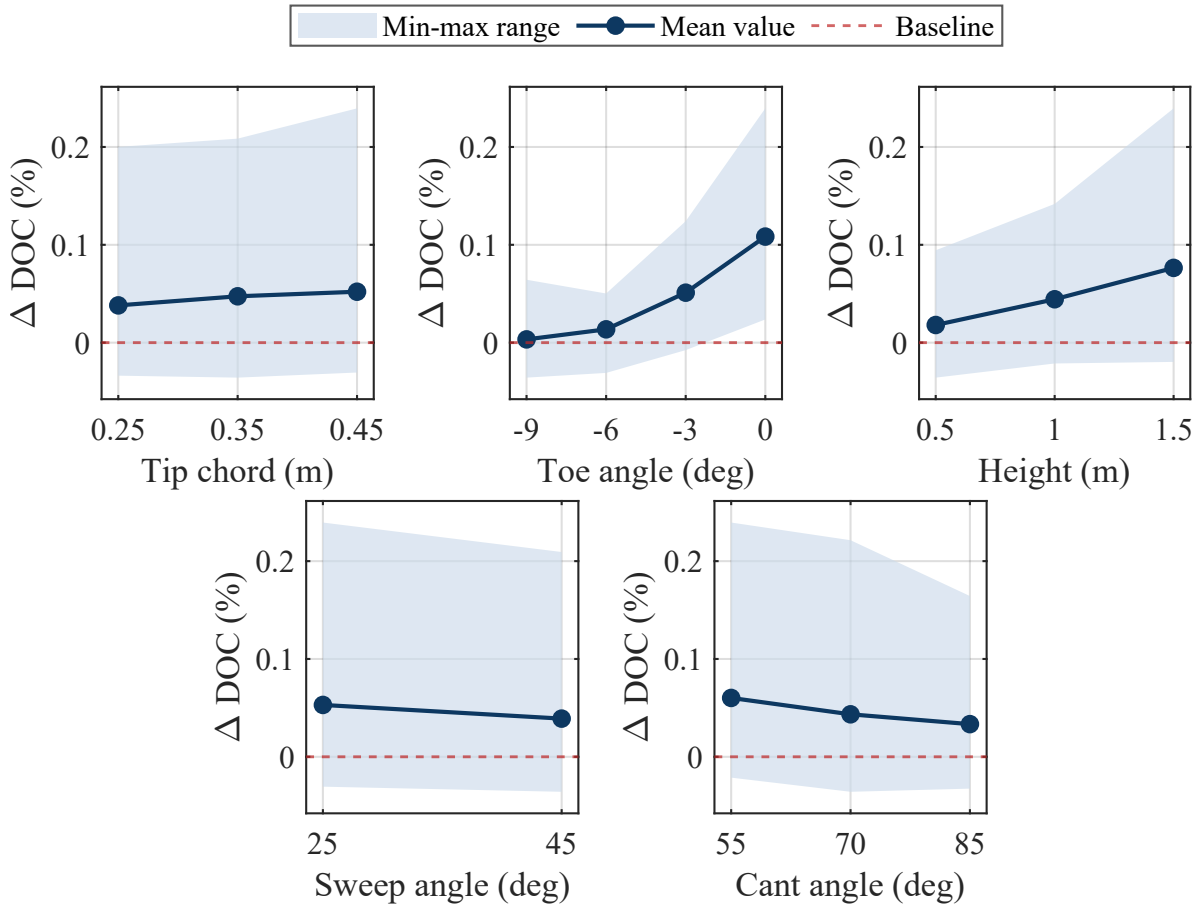


Figure 11 – Main effects of the winglet design variables on DOC variation.

The lowest-DOC winglet configuration therefore improves the baseline, but by an extremely small margin. When model uncertainty is considered together with the additional structural complexity, integration effort, manufacturing implications, and maintenance burden introduced by a winglet, such a margin would not provide a clear justification for modifying the baseline regional aircraft. This outcome is consistent with the physical trade-off expected for regional missions: the cruise segment is not long enough for the induced-drag reduction to translate into a robust economic benefit once structural and operational effects are included.

4. Conclusions

This work presented a cost-driven multidisciplinary framework for the assessment of winglet geometries on a regional aircraft wing. The framework couples parametric geometry generation, panel-method aerodynamic analysis, structural wing-mass estimation, aircraft-level mission performance, and direct operating cost evaluation. The objective is not limited to identifying a locally efficient aerodynamic shape, but rather to determining whether the aerodynamic improvement remains beneficial after structural, mission, and economic effects are propagated to aircraft level.

The application to the reference hybrid-electric regional turboprop shows that winglets can improve local aerodynamic indicators within the explored design space. Reductions in induced-drag factor and increases in maximum lift-to-drag ratio are obtained for several configurations. However, these aerodynamic gains are accompanied by changes in spanwise loading and by a structural mass penalty for the sampled cases. Once the sized wing mass and aerodynamic changes are introduced into the mission and cost models, the aircraft-level benefit becomes marginal.

For the considered mission, the lowest-DOC winglet reduces block fuel by approximately 0.858% and DOC by approximately 0.036% with respect to the baseline aircraft, which confirms that the aircraft-level response is very close to neutral. The benefit is therefore real but marginal, and it remains too

small to support a practical design recommendation, especially when compared with the uncertainty of the aerodynamic, structural, mission, and cost models. The main outcome of the study is therefore that, for the aircraft and regional mission considered here, the addition of a winglet is not economically justified.

This conclusion is consistent with the operating characteristics of regional aircraft. The relatively short cruise segment limits the time over which induced-drag reductions can accumulate, while structural integration complexity and mass-dependent operational penalties reduce the net value of the aerodynamic improvement. The proposed framework remains useful because it makes this trade-off quantitative and traceable across disciplines, rather than relying on aerodynamic performance indicators alone.

Future work will use the same framework to identify the mission and operating conditions for which winglets may become advantageous on regional aircraft. In particular, the effect of range, cruise duration, yearly utilization, energy price, and installation or production cost should be investigated to determine the threshold beyond which the aerodynamic benefit becomes large enough to produce a measurable net economic gain.

5. Contact Author Email Address

The contact author for this paper is Luca Falcone: luca.falcone@unina.it. Additional authors may be reached at: salvatore.corcione@unina.it, fabrizio.nicolosi@unina.it, salvatore.trepiccione@unina.it.

6. Copyright Statement

The authors confirm that they, and/or their company or organization, hold copyright on all of the original material included in this paper. The authors also confirm that they have obtained permission, from the copyright holder of any third party material included in this paper, to publish it as part of their paper. The authors confirm that they give permission, or have obtained permission from the copyright holder of this paper, for the publication and distribution of this paper as part of the ICAS proceedings or as individual off-prints from the proceedings.

7. Acknowledgments

The research presented in this paper has been performed in the framework of the HERA project (Hybrid Electric Regional Aircraft) and has received funding from the European Union Clean Aviation Program under grant agreement n° 101102007.





Co-funded by the European Union



References

[1] Heidari Soreshjani M and Jahangirian A. An investigation on winglet design with limited computational cost, using an efficient optimization method. *Aerospace Science and Technology*, 117:106957, 2021.

[2] Guerrero J, Sanguineti M and Wittkowski K. CFD study of the impact of variable cant angle winglets on total drag reduction. *Aerospace*, 5:126, 12 2018.

[3] Khosravi S and Zingg DW. Aerostructural perspective on winglets. *Journal of Aircraft*, 54(3):1121–1138, 2017.

[4] Bons N, Martins J, Odaguil F and Cuco A. Aerostructural wing optimization of a regional jet considering mission fuel burn. *ASME Open Journal of Engineering*, 1:1–16, 10 2022.

[5] Takenaka K, Hatanaka K, Yamazaki W and Nakahashi K. Multidisciplinary design exploration for a winglet. *Journal of Aircraft*, 45(5):1601–1611, 2008.

[6] Corcione S, Cusati V, Memmolo V, Nicolosi F and Llamas Sandin R. Impact at aircraft level of elastic efficiency of a forward-swept tailplane. *Aerospace Science and Technology*, 140:108461, 2023.

[7] Di Pasquale D and Savill M. The importance of coupling aerodynamic and cost analysis in aircraft design. *CEAS Aeronautical Journal*, 13:1085–1100, 08 2022.

[8] Lappas I and Ikenaga A. Conceptual design and performance optimization of a tip device for a regional turboprop aircraft. *Aerospace*, 6:107, 09 2019.

[9] Elham A and van Tooren MJL. Winglet multi-objective shape optimization. *Aerospace Science and Technology*, 37:93–109, 2014.

[10] Nicolosi F, Corcione S, Trifari V, Cusati V, Ruocco M and Della Vecchia P. Performance evaluation and DOC estimation of an innovative turboprop configuration. In *2018 Aviation Technology, Integration, and Operations Conference*, pages 1–18, Atlanta, Georgia, 2018. American Institute of Aeronautics and Astronautics.

[11] Cusati V, Corcione S, Ciliberti D and Nicolosi F. Design evolution and wind tunnel tests of a three-lifting surface regional transport aircraft. *Aerospace*, 9(3):133, 2022.

[12] Fioriti M, Cabaleiro C, Lefebvre T, Della Vecchia P, Mandorino M, Liscouet-Hanke S, Jeyaraj A, Donelli G and Jungo A. Multidisciplinary design of a more electric regional aircraft including certification constraints. In *AIAA Aviation 2022 Forum*, Chicago, Illinois and Virtual, 2022. American Institute of Aeronautics and Astronautics.

[13] Trifari V, Ruocco M, Cusati V, Nicolosi F and De Marco A. Multi-disciplinary analysis and optimization java tool for aircraft design. In *Proceedings of the 31st Congress of the International Council of the Aeronautical Sciences*, pages 1–11, Belo Horizonte, Brazil, 2018. ICAS2018_0504.

[14] Prakasha PS, Ciampa PD, Della Vecchia P, Ciliberti D, Voskuij M, Charbonnier D, Jungo A, Zhang M, Fioriti M, Anisimov K and Mirzoyan A. Model based collaborative design and optimization of blended wing body aircraft configuration: AGILE EU project. In *AIAA Aviation 2018 Forum*, Atlanta, Georgia, 2018. American Institute of Aeronautics and Astronautics.

[15] Bussemaker JH, Ciampa PD, Singh J, Fioriti M, Cabaleiro De La Hoz C, Wang Z, Peeters DMJ, Hansmann P, Della Vecchia P and Mandorino M. Collaborative design of a business jet family using the AGILE 4.0 MBSE environment. In *AIAA Aviation 2022 Forum*, Chicago, Illinois and Virtual, 2022. American Institute of Aeronautics and Astronautics.

[16] European Union Aviation Safety Agency, Cologne, Germany. *Easy Access Rules for Large Aeroplanes (CS-25), Amendment 27*, 2021. ED Decision 2021/015/R.

[17] European Union Aviation Safety Agency (EASA). *Certification Specifications and Acceptable Means of Compliance for Normal, Utility, Aerobatic and Commuter Category Aeroplanes (CS-23) (Amendment 4)*. European Union Aviation Safety Agency, amendment 4 edition, July 2015. Easy Access Rules online consolidated version published June 2018; Amendment 4 introduced by ED Decision 2015/018/R.

[18] Della Vecchia P, Mirabella C, Tuccillo M, Riboldi CE, Fioriti M, Shahini F and Roncolini F. A SysML-based framework towards EASA CS-23 digitalization: An MBSE approach. *Transportation Research Interdisciplinary Perspectives*, 36:101810, 2026.

[19] Grazioso G, Di Stasio M, Nicolosi F and Trepiccione S. A mathematical model for hybrid-electric propulsion system for regional propeller-driven aircraft. *Energy Conversion and Management: X*, 26:100957, 2025.

[20] Cusati V, Di Stasio M, Lucci G and Zhang Q. Evaluating hybrid-electric aircraft viability: The ampaire eco caravan cost analysis. *Transportation Research Part D: Transport and Environment*, 144:104759, 2025.

[21] Della Vecchia P, Mandorino M, Cusati V and Nicolosi F. Retrofitting cost modeling in aircraft design. *Aerospace*, 9(7):349, 2022.